PNAS RESEARCH ARTICLE | CELL BIOLOGY OPEN ACCESS

Role of Pbr1, a putative oxidoreductase, in the ER quality control and folding of yeast Fks1 glucan synthase

Keisuke Obara[a,1,2], Hiroki Okada[b,c,1], Guihong Tan[d,1], Shinsuke Ohnuki[b], Godai Suzuki[b], Haruka Ohtake[b], Karen Kubo[b], Farzan Ghanegolmohammadi[b], Shunsuke Ishizaka[b], Yoko Yashiroda[e], Aoi Okita[a], Emi Mishiro-Sato[f], Kuninori Suzuki[b], Yasushi Tamura[g], Rei Ashine[h], Yoshiki Ikeda[h], Takumi Kamura[a], Jolanda van Leeuwen[i,j], Brenda Andrews[d], Erfei Bi[c], Nobuo N. Noda[k], Charles Boone[d,e,2], and Yoshikazu Ohya[b,l,m,2]

Affiliations are included on p. 10.

Contributed by Charles Boone; received April 10, 2026; accepted May 21, 2026; reviewed by Jeffrey L. Brodsky and James B. Konopka

The biogenesis of multipass membrane proteins challenges the endoplasmic reticulum (ER) quality control, particularly when transmembrane segments contain polar or charged residues required for function. Fks1, the catalytic subunit of yeast β-(1,3)-glucan synthase, exemplifies this challenge because its large multipass transmembrane architecture must support glucan synthesis at the plasma membrane while also undergoing efficient biogenesis in the ER. Here, we investigate the cellular role of *PBR1* (*YNL181W*), an essential gene whose role remains uncharacterized even though its predicted product has similarity to oxidoreductases. By integrating quantitative morphological profiling with global genetic interaction analysis, we found that *PBR1* function converges on cell-wall biosynthesis and closely parallels that of *FKS1*. Partial loss of Pbr1 function caused temperature-sensitive growth defects but also impaired β-(1,3)-glucan synthesis, and weakened cell-wall integrity. Under these conditions, Fks1 failed to accumulate at the cell surface and, instead, accumulated in ER-associated compartments, where it exhibited reduced stability. Biochemical analyses revealed the accumulation of immature Fks1 species, including forms defective in glycosylation, consistent with compromised ER quality control. A spontaneous missense suppressor allele of *FKS1* partially restored Fks1 stability and growth, supporting a functional relationship between the two proteins. Pbr1 is a cytosol-facing ER membrane protein that physically associates with Fks1, and structural modeling suggests that it adopts a Rossmann-like fold capable of binding pyridine nucleotides despite divergence from canonical catalytic motifs. Together, these findings identify Pbr1 as an ER-associated, chaperone-like factor required for the folding and maturation of Fks1.

yeast | ER quality control | glucan synthase

Significance

The budding yeast genome has long served as a foundation for understanding eukaryotic cell biology, yet a small number of essential genes have resisted functional assignment. *PBR1* is one such gene: although its sequence suggested similarity to oxidoreductases, its molecular role remained unclear. Here, genome-scale functional analyses have revealed that *PBR1* function converges on cell-wall biosynthesis and closely parallels that of *FKS1*, a multipass β-(1,3)-glucan synthase. We show that Pbr1 operates at the endoplasmic reticulum (ER) to support the folding and stability of Fks1, enabling proper cell-wall assembly. By resolving the function of a long-standing essential gene, this work reveals an ER quality-control mechanism that enables constrained membrane proteins to fold efficiently and perform essential cellular functions.

Transmembrane (TM) proteins must attain precise folding and insertion into biological membranes to achieve accurate topological and functional configuration. Most TM domains traverse the lipid bilayer as α-helical segments enriched in hydrophobic residues. Single-pass membrane proteins whose N termini face the cytosol encounter a unique topological constraint: their TM helices must undergo inversion within the endoplasmic reticulum (ER) membrane to achieve the correct orientation. Similarly, during the biogenesis of multipass membrane proteins, alternate TM segments must adopt inverted topologies. The orientation of TM helices is determined by intrinsic biophysical parameters, including their length, hydrophobicity, and the distribution of charged or polar residues within the helix, or at the cytosol–membrane interfacial boundary (1–4).

The misfolding of TM proteins is implicated in the etiology of numerous human diseases. For example, cystic fibrosis arises from misassembly of the CFTR chloride channel, Niemann-Pick disease from conformational defects in the NPC1 cholesterol transporter, and retinitis pigmentosa from structural destabilization of the rhodopsin photoreceptor (5–7). In many such cases, single–amino acid substitutions within TM segments—particularly hydrophobic-to-polar or charged replacements—perturb helix stability, resulting in protein aggregation or loss of proteostasis (8, 9).

Hydrophobic α-helices spontaneously embed in the nonpolar core of the lipid bilayer, yet exposure to the aqueous cytosol predisposes them to structural destabilization and aggregation. Conversely, membrane proteins that mediate translocation of polar substrates, such as transporters and channels, must strategically position hydrophilic residues within TM helices to form aqueous translocation conduits (10). A prototypical example is Fks1, a multipass plasma membrane glycosyltransferase responsible for synthesizing and exporting β-(1,3)-glucan, a principal structural polymer of the yeast cell wall (11, 12). The

Reviewers: J.L.B., University of Pittsburgh; and J.B.K., Stony Brook University.

The authors declare no competing interest.

[1]K.O., H.O., and G.T. contributed equally to this work.

[2]To whom correspondence may be addressed. Email: obara.keisuke.r2@f.mail.nagoya-u.ac.jp, charlie.boone@utoronto.ca, or ohya@vos.nagaokaut.ac.jp.

This article contains supporting information online at https://www.pnas.org/lookup/suppl/doi:10.1073/pnas.2612792123/-/DCSupplemental.

Published July 13, 2026.

biological and clinical importance of Fks1 is underscored by the fact that β-(1,3)-glucan synthase is the target of echinocandins, including caspofungin, whose inhibitory interaction with Fks1 has recently been resolved structurally (13). Cryoelectron microscopy revealed that Fks1 spans the membrane with 17 TM helices, forming a channel for glucan translocation (11). Especially because these membrane spanning domains contain a number of hydrophilic amino acids within the channel, the correct folding and assembly of such complex multipass TM proteins pose a formidable cellular challenge. Eukaryotic cells have therefore evolved an intricate ER–associated proteostasis network that facilitates co- and posttranslational folding (14). In yeast, the small TM protein Ilm1 appears to act as a specialized molecular chaperone that promotes the cotranslational folding of nascent Fks1 polypeptides (15). Ilm1 functions cooperatively with the highly conserved ER membrane protein complex (EMC)—an octameric assembly (Emc1–6, Sop4, and Emc10)—that coordinates the membrane insertion and topogenesis of multipass TM proteins (15, 16). Consistent with this functional relationship, Fks1 and Ilm1 were identified together with multiple EMC components in an Emc3 coimmunoprecipitation and mass spectrometry analysis (15). Notably, the same Ilm1 coimmunoprecipitation experiment also recovered Pbr1 (Ynl181w) (15).

Here, we functionally delineate *PBR1*, one of the few remaining uncharacterized essential genes in *Saccharomyces cerevisiae*. *PBR1* encodes a putative ER-resident oxidoreductase with a Rossmann-like fold. By integrating genetic, cell biological, and biochemical analyses, we uncover a previously unappreciated role for Pbr1 in ER quality control during the biogenesis of multipass membrane proteins.

Results

PBR1 Morphological Profile. To systematically probe *S. cerevisiae* gene function, we analyzed a comprehensive collection of temperature-sensitive (ts) and gene-deletion mutants. Each strain was cultured at a semipermissive temperature, imaged by fluorescent microscopy, and quantified for 501 morphological parameters using CalMorph (17). A generalized linear model was then applied to extract morphological trait values for each mutant and generate morphological profiles (MPs). We next compared the profile of each target mutant to all the other ts and deletion strains to identify genes sharing similar MPs. Genes with highly correlated profiles were inferred to act in the same biological processes (18), and these relationships were visualized as a correlation network.

The *PBR1* profile showed significant MP correlations (FDR = 0.05, Fisher's exact test) with genes involved in several cell-wall biosynthetic pathways. The strongest enrichment was for GO:0042546 and GO:0016757 ($P = 2.7 \times 10^{-6}$), encompassing β-(1,6)-glucan biosynthesis, *N*-linked glycosylation, and glycosylphosphatidylinositol (GPI)-anchor synthesis (Fig. 1*A*) (19, 20). These results suggest that *PBR1* contributes somehow to cell-wall maintenance. Comparison of the *PBR1* MP with those of all nonessential gene-deletion mutants revealed a significant morphological similarity between *PBR1* and *FKS1*, a key gene in β-(1,3)-glucan biosynthesis (Fig. 1*B*). Together, these data indicate that *PBR1* plays a central role in yeast cell-wall biosynthesis.

PBR1 Genetic Interaction Profile. Global yeast genetic interaction mapping provides another unbiased approach for identifying genes with similar functions (21). In this analysis, mutant alleles of specific query genes were crossed to the set of ~5,000 nonessential gene deletion mutants and a set of ~870 conditional, essential gene ts mutants (screened at a semipermissive temperature), and the resultant double mutants were scored for both negative and positive genetic interactions (21). Previously, we constructed 6 different *pbr1* ts alleles by error prone PCR, generating alleles with 2 to 4 amino acid substitutions (*SI Appendix*, Fig. S1 *A* and *B* and Table S1). A global analysis of yeast genetic interactions (21) revealed that all of the *pbr1* ts alleles showed a similar pattern of genetic interactions (Fig. 1*C*). For example, *pbr1* ts alleles displayed negative genetic interactions with different genes and their corresponding pathways, including 1) components of the *PKC1* kinase pathway, which controls cell wall remodeling and polarized cell growth during budding and mating, 2) *CNB1*, encoding the regulatory subunit of calcineurin, a calmodulin-regulated type 2B protein phosphatase that governs the Crz1-mediated cell wall stress response, 3) the *CHS3* cell wall chitin synthesis pathway (19), 4) genes encoding the EMC subunits, which coordinates the membrane insertion of multipass TM proteins.

PBR1 also showed positive genetic interactions with several genes involved in the β-(1,6)-glucan biosynthetic process, *N*-linked glycosylation, GPI-anchor synthesis, and sphingolipid biosynthesis (Fig. 1*C*). These relatively weak positive interactions indicate that the growth defects caused by perturbation of these pathways are either captured or buffered in the *pbr1* mutant background.

Genes that display highly similar genetic interaction profiles often share a coordinated functional relationship. The *pbr1* mutants exhibited high profile similarity with each other and with the *fks1*Δ mutant (Fig. 1*D*), suggesting *PBR1* and *FKS1* may operate in a shared functional context related to β-(1,3)-glucan synthesis. We also found that *smi1*Δ and *ilm1*Δ mutants showed genetic interaction profile similarity that overlapped with that of *pbr1* mutants (Fig. 1*D*). Like *fks1*Δ mutants, *smi1*Δ cells are known to have reduced β-(1,3)-glucan synthesis activity (20). Ilm1 appears to function as a molecular chaperone that collaborates with the EMC complex in the cotranslational folding of Fks1 (15). These findings place Pbr1 within the functional network governing Fks1 and β-(1,3)-glucan synthesis. To dissect *PBR1* function in more detail, we focused on the analysis of three ts alleles, *pbr1-5014*, *pbr1-5002*, and *pbr1-5006* (*SI Appendix*, Fig. S1 *A*–*C*).

Isolation of a Spontaneous Suppressor of the pbr1-5006 Mutant. To further explore the role of *PBR1*, we isolated a spontaneous, extragenic suppressor mutant of the temperature sensitivity of *pbr1-5006* (*SI Appendix, Supplementary Materials and Methods*). Genetic suppressors are rare examples of strong positive genetic interactions that can identify genes whose products work in the same functional module and may interact physically (21). Tetrad analysis showed that the suppression was mediated by a single gene. Subsequent genetic mapping (22) and whole-genome sequencing identified a missense mutation in *FKS1*, resulting in a single–amino acid substitution, Fks1-A768D. The suppression phenotype associated with the *fks1-A768D* allele cannot bypass the lethality of a *pbr1*Δ deletion allele, indicating that *pbr1-5006* remains partially functional at the restrictive temperature. Moreover, tetrad analysis showed that the genetic suppression phenotype is allele specific (*SI Appendix*, Fig. S1*D*). The *FKS1-PBR1* genetic suppression interaction provides additional evidence suggesting that Pbr1 may be particularly important for establishing Fks1 function.

β-(1,3)-Glucan Synthesis Is Perturbed in pbr1 Mutants. We analyzed the cell wall of *pbr1* ts mutants using multiple assays. Cell-wall integrity was evaluated by calcofluor white (CW) sensitivity. CW binds strongly to chitin, and mutants with weakened cell

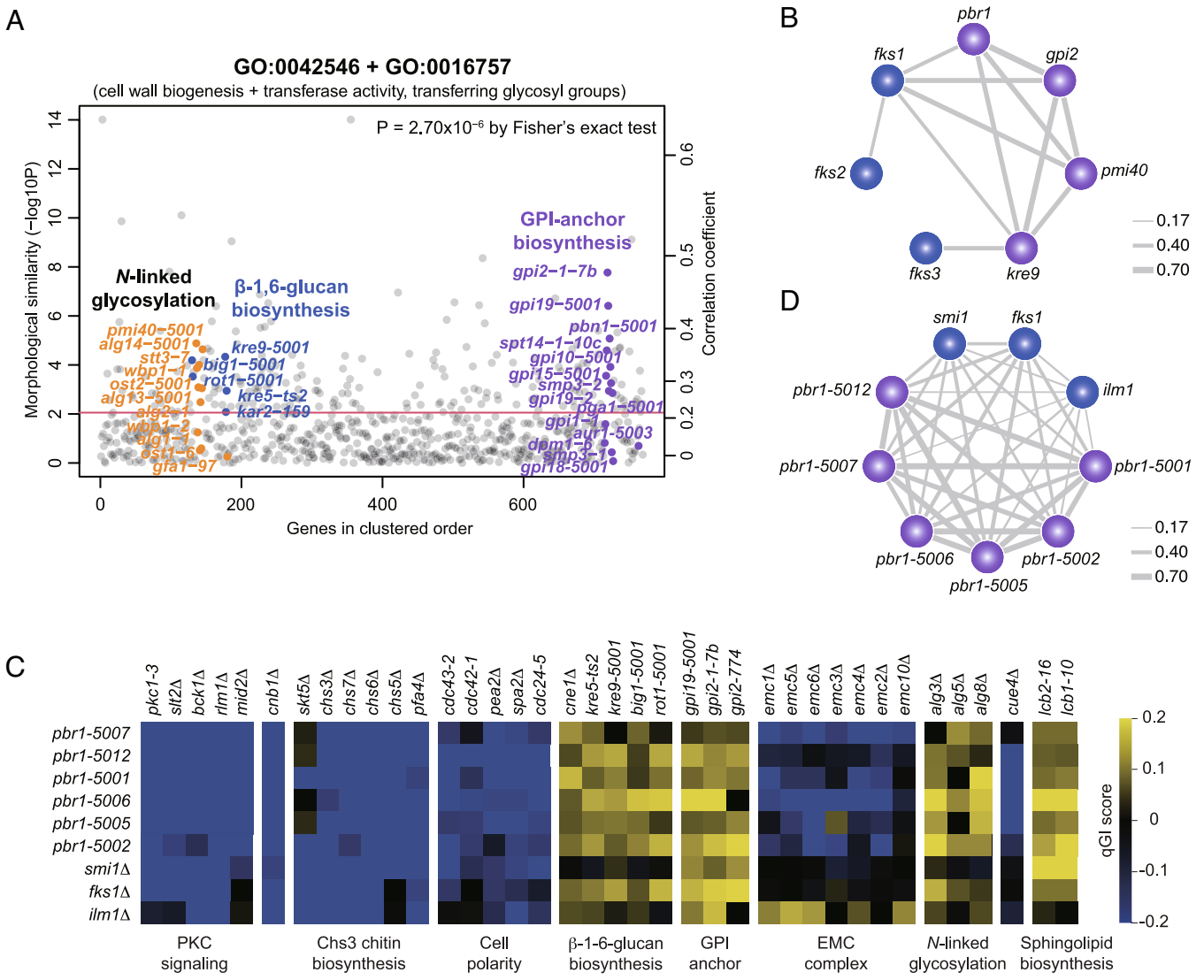

Fig. 1. Morphology-based profiling and genetic interaction mapping highlight a close relationship between *PBR1* and *FKS1*. (*A*) Morphological profile of *pbr1-5014* was significantly correlated with subsets of genes annotated to GO:0042546 and GO:0016757 in multiple cell-wall biosynthetic pathways. Orange, blue, and purple dots highlight mutants of the annotated genes defective in *N*-linked glycosylation, β-(1,6)-glucan biosynthesis, and GPI-anchor synthesis, respectively. The red horizontal line indicates the significance threshold (FDR = 0.01, two-tailed *t* test for correlation coefficient). *P* value of Fisher's exact test indicates significance for an enrichment of the highlighted mutants in the significantly correlated mutants with *pbr1-5014* at FDR = 0.01 by the one-tailed *t* test. (*B*) Correlation network showing that *pbr1-5014* clusters with glucan synthase (*fks1, fks2, fks3*), *N*-glycosylation (*pmi40-5001*), and GPI-anchor synthesis (*gpi2-1-7b*) mutants. (*C*) Heatmap of quantitative genetic interaction scores for selected double mutant. Negative interactions are shown in blue and positive interactions in yellow. Query gene mutants are indicated on the y-axis and array gene mutants are grouped according to function and indicated on the *x*-axis. (*D*) Genetic interaction profile similarity network. Genes (purple and blue nodes) that share similar genetic interaction profiles are connected by a gray edge. The thickness of the edge in (*B* and *D*) reflects the morphological similarity and genetic interaction profile similarity, respectively, as measured by Pearson's Correlation coefficient, as described elsewhere (17, 21).

walls display hypersensitivity, which serves as a classical indicator of cell-wall defects (23, 24). We found marked hypersensitivity in all *pbr1* mutants tested, but not in the *pbr1-5006 fks1-A768D* suppressor (*SI Appendix*, Fig. S2*A*). CW staining was also more intense than in wild-type (WT) cells, resembling the *fks1-1154* mutant (Fig. 2*A*), likely reflecting chitin accumulation in a weakened wall. Together, these observations indicate that *pbr1* mutations compromise cell-wall integrity.

We next examined β-(1,3)-glucan using aniline blue, which preferentially stains β-(1,3)-glucan in the yeast cell wall. The fluorescence signal was weaker in *pbr1* mutants than in WT, particularly at the bud, where wall synthesis is normally active (Fig. 2*B*). Quantification of cells showing visibly reduced bud signal confirmed that this phenotype was significantly more frequent in *pbr1* mutants ($P < 0.01$, Student's *t* test; Fig. 2*C*). This phenotype mirrors that of the β-(1,3)-glucan–deficient *fks1-1154* strain, suggesting that Pbr1 is required for efficient β-(1,3)-glucan synthesis. Consistently, in vitro β-(1,3)-glucan synthase activity in membrane fractions from *pbr1* mutants was significantly reduced relative to WT ($P < 0.05$, Student's *t* test; Fig. 2*D*).

Notably, the ts growth of *pbr1* mutants was rescued by sorbitol, a common osmotic stabilizer that protects cell-wall–defective strains, including those with impaired Rho1-dependent activation of Fks1 (25) (*SI Appendix*, Fig. S2*A*).

Finally, electron microscopy revealed that the β-(1,3)-glucan layer was significantly thinner in *pbr1* mutants than in WT (*SI Appendix*, Fig. S2 *B* and *C*; $P < 0.05$, Student's *t* test). Collectively, these results demonstrate that Pbr1 is essential for β-(1,3)-glucan synthesis and cell-wall assembly, and that defects in this process underlie the ts phenotype of *pbr1* mutants.

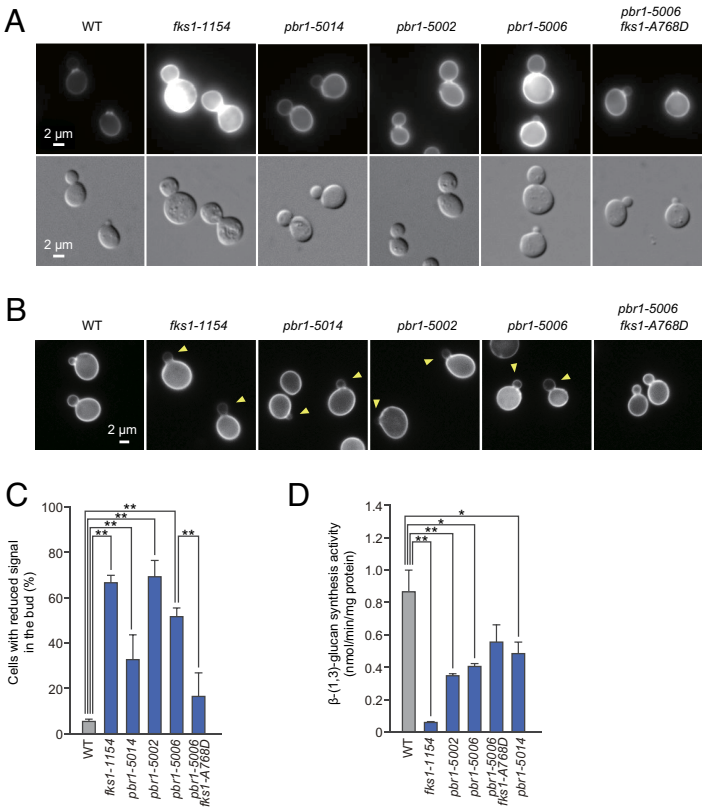

Fig. 2. *pbr1* mutants have defective cell wall. (*A*) Calcofluor white (CW) fluorescence images (top) and differential interference contrast (DIC) images (bottom) of yeast cells. Cells were shifted from 25 °C to 37 °C for 4 h and then stained with CW. Fluorescence microscopy shows stronger CW staining in *pbr1* mutants compared with WT. (*B*) Aniline blue (AB) staining of the yeast cells. Cells in log phase were stained with AB and observed by fluorescence microscopy. The arrowheads indicate reduced AB signal in the bud. (*C*) Percentage of cells with reduced AB signal in the bud. Cells were scored as having reduced bud signal when AB fluorescence in the bud was visibly weaker than that in the mother-cell wall within the same cell. Values represent mean ± SD from three independent experiments. $^{**}P < 0.01$ (Student's *t* test). (*D*), β-(1,3)-glucan synthesis activity in the membrane fraction was measured. Values represent the mean ± SEM from three independent experiments. $^{*}P < 0.05$, $^{**}P < 0.01$ (Student's *t* test).

Fks1 Is Mislocalized to the ERAC in pbr1 Mutants. Because *pbr1* mutants exhibit reduced β-(1,3)-glucan synthesis, we examined whether the subcellular localization of Fks1 was altered. In WT cells, GFP–Fks1 was primarily detected at the plasma membrane of the bud, where cell-wall synthesis occurs, at both 25 °C and 37 °C (Fig. 3*A*). In contrast, the bud-localized signal was markedly weaker in *pbr1* ts mutants, particularly at 37 °C (Fig. 3 *A* and *B*). Importantly, this defect was rescued in the *pbr1-5006 fks1-A768D* suppressor mutant, indicating that partial loss of Pbr1 function leads to Fks1 mislocalization.

Because punctate intracellular structures appeared concomitantly with the loss of the bud signal (Fig. 3*C*), we reasoned that Fks1 might be trapped within the secretory pathway, likely in the ER or Golgi. The ER-associated compartment (ERAC) is a peri-ER structure in which misfolded proteins accumulate for ER-associated degradation (ERAD) (26). Colocalization analysis revealed that the GFP–Fks1 puncta overlapped with mCherry–Hlj1, an ERAC marker (Fig. 3*D*), confirming that Fks1 accumulates in the ERAC of *pbr1* mutants.

We next asked whether other ER quality-control factors produce similar phenotypes. Among them, *ILM1*, which displays a genetic interaction profile similar to *PBR1*, was a prime candidate. In *ilm1*Δ cells, GFP–Fks1 signals at the bud were reduced and instead accumulated in intracellular puncta reminiscent of the ERAC, although less pronounced than in *pbr1* mutants (Fig. 3 *E* and *F*). Deletion of *EMC6*, *SOP4*, or *CUE4*—encoding a core EMC subunit, a peripheral subunit, and a ubiquitin-binding ER protein that copurifies with Ilm1—caused a milder but detectable reduction in bud-localized Fks1 (Fig. 3 *E* and *F*).

Together, these findings indicate that Pbr1 and other ER quality-control factors cooperate to ensure the proper folding and trafficking of Fks1, and that disruption of this process leads to its retention within the ERAC, where it is likely targeted for ERAD-mediated degradation.

Pbr1 Stabilizes Fks1 by Promoting Its Maturation in the ER. Fluorescence microscopy suggested that in *pbr1* mutants, Fks1 accumulates in the ERAC. To confirm this at the protein level, we compared cellular Fks1 abundance between WT and *pbr1* mutants by immunoblotting. Fks1 levels were significantly reduced ($P < 0.01$, Student's *t* test) in *pbr1* cells at both 26 °C and 37 °C (Fig. 4 *A* and *B*). In the *pbr1-5006 fks1-A768D* suppressor mutant, Fks1 levels were partially restored relative to the parental *pbr1-5006* strain (Fig. 4 *A* and *B*), consistent with its improved growth at 37 °C.

Additional bands with higher electrophoretic mobility appeared in *pbr1* mutants and were designated as Fks1′ (arrowheads in Fig. 4*A*) and Fks1″ (arrows in Fig. 4*A*). These forms accumulated in *pbr1-5002 hrd1*Δ *doa10*Δ cells, which lack the E3 ubiquitin ligases required for the ERAD. This observation indicates that loss of Pbr1 leads to incomplete maturation of Fks1 in the ER, and suggests that these immature species are normally eliminated via the ERAD pathway.

To determine whether the altered electrophoretic mobility of Fks1 in *pbr1* mutants reflects defective glycosylation, we analyzed both *N*- and *O*-linked modifications. Endo H digestion caused a slight downshift of Fks1 bands, confirming that Fks1 is normally *N*-glycosylated (*SI Appendix*, Fig. S3*A*). Inhibition of *O*-glycosylation

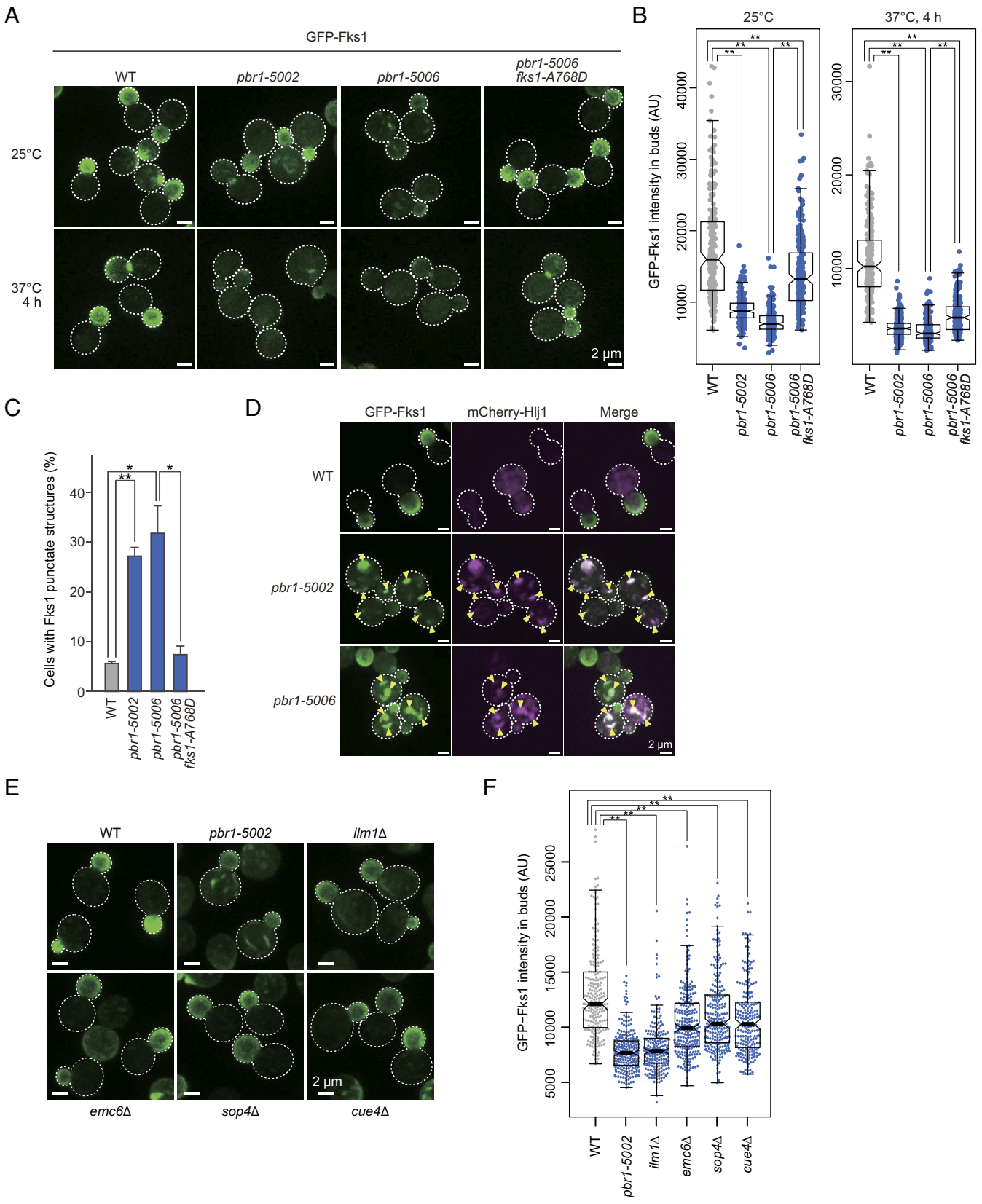

Fig. 3. Fks1 is sequestered to the ERAC in *pbr1* mutants. (*A*) Localization of GFP-Fks1 in WT, *pbr1-5002*, *pbr1-5006*, and *pbr1-5006 fks1-A768D* cells at 25 °C and after 4 h at 37 °C. (*B*) Quantification of GFP-Fks1 intensity in the bud region from (*A*). Box plots show distribution of >190 cells from three independent experiments. (*C*) Cells were grown and imaged at 25 °C. Percentage of cells with intracellular punctate GFP-Fks1 structures. Values represent mean ± SD of >320 cells from three independent experiments. (*D*) Colocalization of GFP-Fks1 (green) with the ERAC marker mCherry-Hlj1 (magenta). Arrowheads indicate GFP-Fks1 accumulation at the ERAC at 25 °C. (*E*) Localization of GFP-Fks1 in *pbr1-5002* and ER quality-control mutants (*ilm1*Δ, *emc6*Δ, *sop4*Δ, *cue4*Δ) at 25 °C. (*F*) Quantification of GFP-Fks1 intensity in the bud region from (*E*). *$P < 0.05$, **$P < 0.01$ [Student's *t* test; for (*B*, *C*, and *F*)].

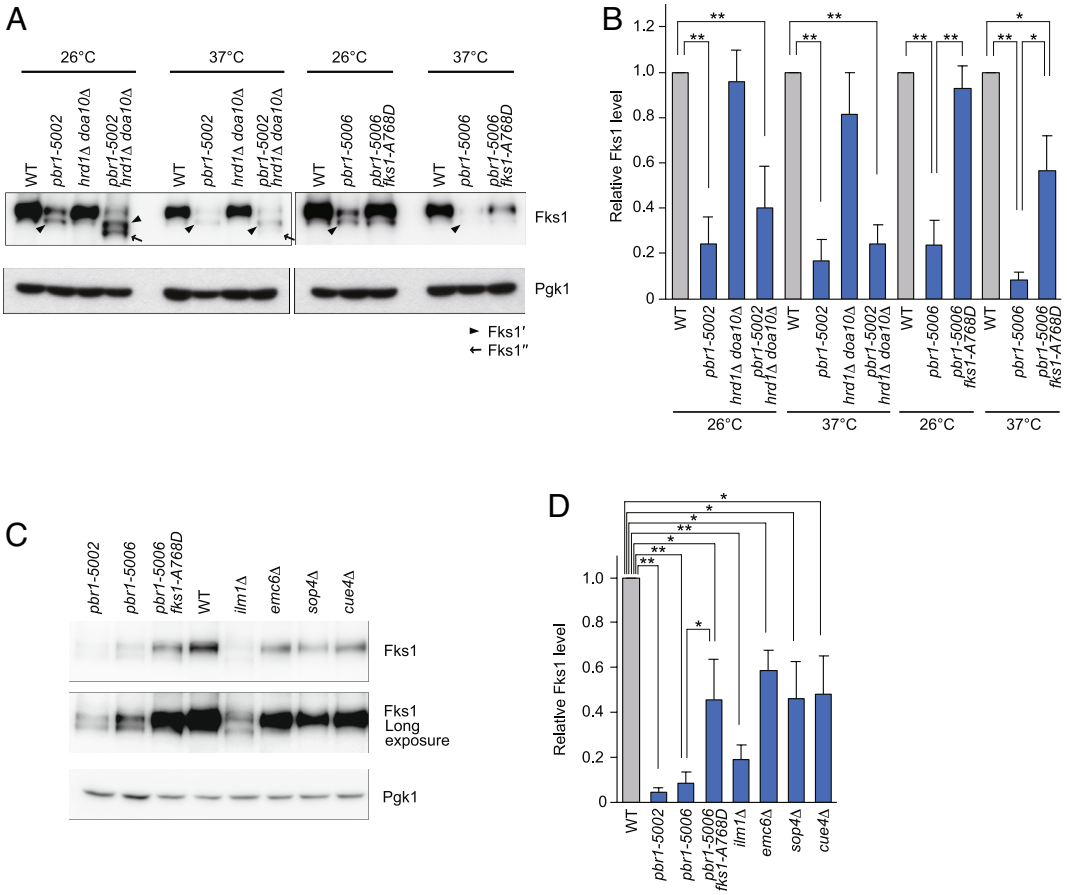

Fig. 4. Fks1 level is reduced in *pbr1* and the EMC mutants. (*A*) Levels of Fks1 and Pgk1, a loading control protein, in WT and *pbr1* mutants. Cells were cultured to log phase and harvested at 26 °C and 2 h at 37 °C. Arrowheads / arrows indicate the second band seen in lysates of *pbr1* mutants / the third band seen in *pbr1-5002 hrd1*Δ *doa10*Δ lysate. (*B*) Fks1 levels were normalized with those of Pgk1 and shown as a relative value to WT. (*C*) Levels of Fks1 and Pgk1 in WT and indicated mutants grown to log phase at 26 °C. (*D*) Fks1 levels were normalized and shown as in (*B*). In (*B* and *D*) values represent the mean ± SD from three independent experiments. **P* < 0.05, ***P* < 0.01 (Student's *t* test).

with R3A-5a (27, 28) produced a band identical to Fks1′ observed in untreated *pbr1-5002* cells, indicating that Fks1′ corresponds to an *O*-glycosylation–defective form (*SI Appendix*, Fig. S3 *A* and *B*). Blocking both *N*- and *O*-glycosylation generated a faster-migrating band identical to Fks1″, also seen in *pbr1-5002 hrd1*Δ *doa10*Δ cells (Fig. 4*A* and *SI Appendix*, Fig. S3 *A* and *B*). *N*- and *O*-glycosylation have been implicated in the correct folding of proteins and, thereby, in ER quality control (29, 30). Notably, when glycosylation of Fks1 was inhibited by R3A-5a or tunicamycin, the protein was no longer retained in the ERAC but instead trafficked to the vacuole and cell surface (*SI Appendix*, Fig. S4 *A* and *B*). This behavior differs from that of *pbr1-5002* cells, in which Fks1 accumulates within the ERAC (Fig. 3*D*). Therefore, the ERAC localization of Fks1 in *pbr1-5002* is not simply a consequence of defective glycosylation. Rather, Pbr1 likely facilitates proper maturation of Fks1 within the ER, ensuring its stability and accurate trafficking.

Finally, in *ilm1*Δ cells, Fks1 levels were markedly reduced, accompanied by an *O*-glycosylation defect similar to that observed in *pbr1* mutants (Fig. 4 *C* and *D*). Together, these findings demonstrate that Pbr1 promotes the maturation and stability of Fks1 in the ER by facilitating its proper quality control.

Fks1 Transmembrane Helices Are Enriched in Charged Residues. Nascent Fks1 synthesized at the ER membrane is unstable in *pbr1* mutant cells. To explore the molecular basis of this instability, we analyzed the amino acid composition of its transmembrane (TM) regions (11). Several TM helices of Fks1 were found to be enriched in charged and polar residues (Fig. 5*A* and *SI Appendix*, Fig. S5*A*). This enrichment likely reflects Fks1 function in translocating β-(1,3)-glucan chains across the plasma membrane, yet it may simultaneously complicate TM folding within the ER.

The cytosolic region following the 6th TM helix contains residue A768 (Fig. 5*A*) and substitution of this residue with Asp (A768D) suppresses the temperature sensitivity of the *pbr1-5006* mutant. A768 lies within a short coil region between two conserved α-helices (*SI Appendix*, Fig. S5*B*). Structural prediction suggests that the A768D substitution induces only local conformational changes while increasing the negative charge of the short coil region (*SI Appendix*, Fig. S5*C*).

Pbr1 Is Inserted Into the ER Membrane from the Cytosolic Side. Pbr1 is predicted to contain a single hydrophobic helix (Fig. 5*B* and *SI Appendix*, Fig. S1*A*). C-terminally tagged Pbr1–GFP colocalized with the ER marker Sec61–mCherry (*SI Appendix*, Fig. S1*E*) (34–38). We examined Pbr1 topology in the context of a C-terminally tagged auxin-inducible degron (AID) fusion protein, Pbr1–HA–AID, which partitioned into the membrane fraction and was solubilized by Triton X–100 but not by high concentrations of NaCl or urea, indicating that Pbr1 is an integral membrane protein (Fig. 5*C*). We found that both N- and C-terminally AID-tagged Pbr1 proteins were efficiently degraded in the presence of auxin (Fig. 5*D*), demonstrating that both termini are exposed to the cytosol, indicating that Pbr1 is a cytosol-facing

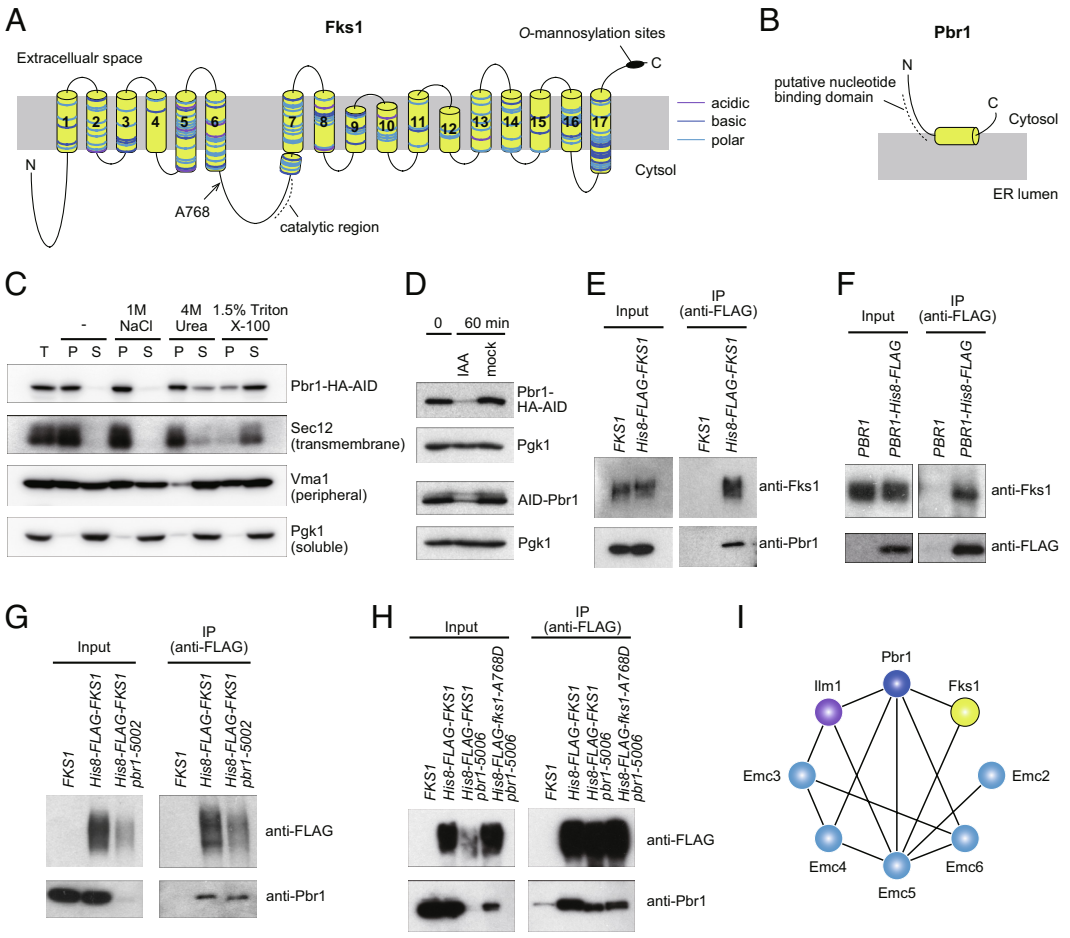

Fig. 5. Pbr1 is inserted into the ER membrane and physically interacts with Fks1. (*A*) Schematic diagram of the membrane topology of Fks1 (11, 31, 32). Acidic, basic, and polar residues within transmembrane (TM) helices are shown in purple, blue, and light blue, respectively. (*B*) Schematic diagram of Pbr1. (*C*) Biochemical fractionation of chromosomally expressed Pbr1–HA–AID under the control of its native promoter. T, total lysate; P, pellet fraction after ultracentrifugation at 100,000× *g*; S, supernatant fraction after ultracentrifugation at 100,000× *g*. (*D*) Auxin-inducible degron analysis of Pbr1–HA–AID and AID–Pbr1 (33). Efficient degradation upon treatment with auxin [indole-3-acetic acid (IAA)] indicates that both the N and C termini of Pbr1 are exposed to the cytosol. (*E*–*H*) Cells were cultured to log phase at 26 °C and subjected to coimmunoprecipitation analysis. (*I*) Summary of the protein–protein interaction network revealed by integrated membrane yeast two-hybrid analysis.

ER membrane protein anchored by a single hydrophobic helix that is embedded in the ER membrane.

Pbr1 Forms a Complex with Fks1. We found that Pbr1 coprecipitated with His_8–FLAG–Fks1 and vice versa (Fig. 5 *E* and *F*). However, only a small fraction of Pbr1 was copurified with Fks1, suggesting that the interaction is transient.

In *pbr1-5002* cells, both His_8–FLAG–Fks1 and Pbr1-5002 levels were markedly reduced (Fig. 5*G* and *SI Appendix*, Fig. S1 *F* and *G*), yet the amount of Pbr1-5002 coimmunoprecipitated with His_8–FLAG–Fks1 was comparable to that of WT Pbr1 in WT cells (Fig. 5*G*). A similar pattern was observed in *pbr1-5006* cells, where His_8–FLAG–Fks1 exhibited stronger binding to Pbr1-5006 than to WT Pbr1 (Fig. 5*H*). These enhanced interactions suggest that Pbr1 preferentially associates with folding-impaired Fks1 species, consistent with a chaperone-like role.

A network of Pbr1 protein interactions involving Fks1, Ilm1, and the EMC complex. To examine the possibility of a network of interactions among Pbr1, Fks1, Ilm1, and components of the EMC complex, we employed the integrated membrane yeast two-hybrid (iMYTH) assay (39, 40). We constructed iMYTH bait fusions for three genes whose products have cytosolic C termini, including *PBR1*, *EMC3,* and *EMC5*, whereas iMYTH prey fusions were constructed for six genes whose products have cytosolic N termini, including *PBR1*, *ILM1*, *EMC2*, *EMC4*, *EMC6*, and *FKS1*. These iMYTH assays recapitulated the Pbr1–Fks1 interaction (*SI Appendix*, Fig. S6), and highlighted a highly interconnected network of interactions among Pbr1, Ilm1, Fks1, and EMC complex components as shown in Fig. 5*I*.

Structural Analysis and Modeling of the Pbr1–Fks1 Interaction. The tertiary structure of Pbr1 was predicted using the AlphaFold3 program (41). Sequence and structural analyses indicated that Pbr1 consists of a Rossmann-like fold, a structural motif frequently found in nucleotide-binding proteins, and a hydrophobic helix domain that interacts with the membrane, from which both N- and C-terminal helices extend (Fig. 6*A*). In contrast, the structure of Fks1 (11) comprises 17 TMs and two cytoplasmic domains: a catalytic glycosyltransferase (GT) domain and an N-terminal accessory (AC) domain. When the predicted structure of Pbr1 and Fks1 were subjected to AlphaFold-Multimer analysis, the AC domain of Fks1 was found to interact with the Rossmann-like fold side of Pbr1 (Fig. 6*B*). However, in the model including full-length Fks1, steric clashes were observed, as the TM and GT domains of Fks1 overlapped the position of Pbr1 (*SI Appendix*, Fig. S7*A*).

To validate this structural model, we employed a system in which a TurboID tag, which labels proteins within ~10 nm of the fusion site (42), was fused to the C terminus of Pbr1 (*SI Appendix*,

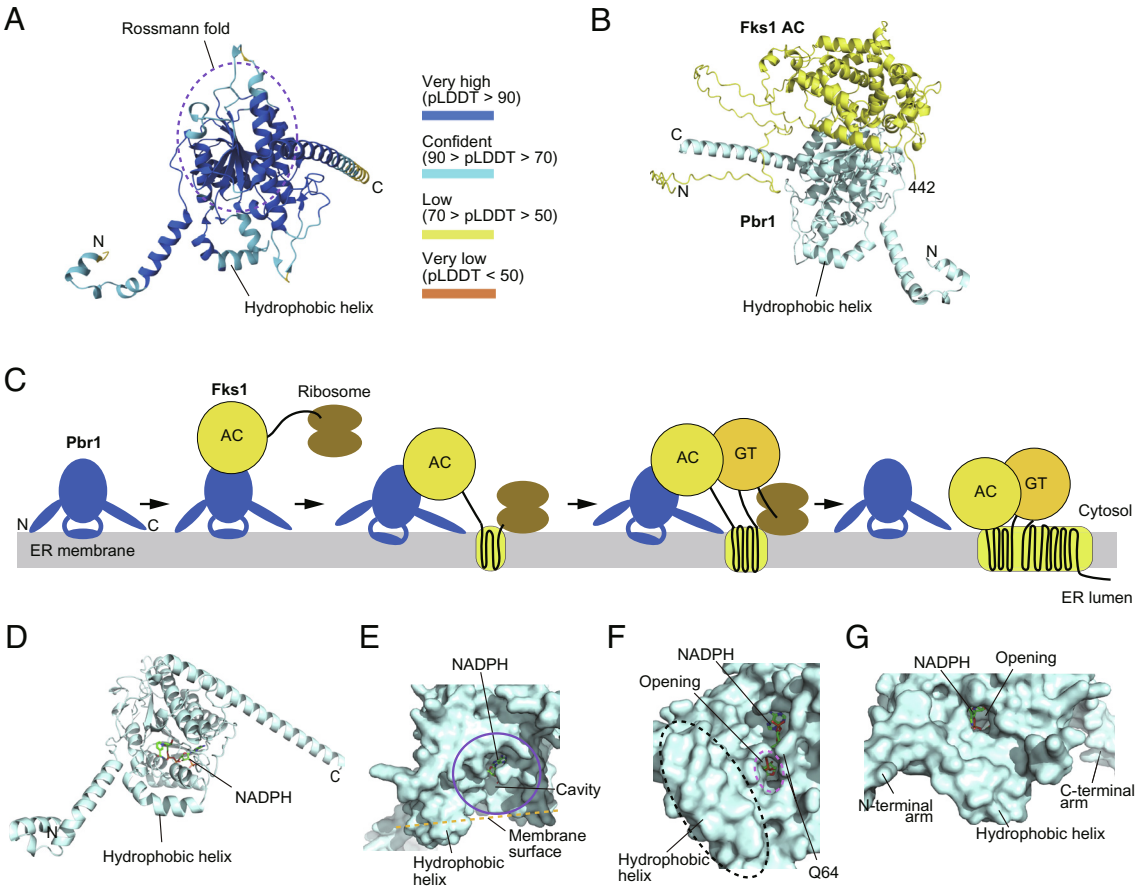

Fig. 6. Structural modeling of Pbr1 and its interaction with Fks1. (*A*) Structure of Pbr1 was predicted using AlphaFold3 (AF3) (41). Coloring indicates the predicted local distance difference test (pLDDT) confidence score. (*B*) A structural model of Pbr1 (cyan) in complex with the accessory (AC) domain of Fks1 (yellow) (11), generated by AlphaFold-Multimer and visualized using PyMOL (http://www.pymol.org). (*C*) A working model for how Pbr1 assists Fks1 biogenesis at the ER membrane. The N-terminal AC domain of Fks1 engages Pbr1 during early stages of translation. As synthesis of the remaining regions proceeds adjacent to Pbr1, folding is facilitated, followed by dissociation of the two proteins during or after completion of Fks1 synthesis. GT, glycosyltransferase domain. (*D*) The Rossmann-like fold of Pbr1 is predicted to accommodate NADPH. (*E*) The cavity of the Rossmann-like fold is oriented toward the membrane surface. (*F*) View of the cavity entrance shown in (*E*) from the membrane-facing side. (*G*) An additional opening is visible at the back of the pocket when viewed from the opposite side of (*E*).

Fig. S7*B*). In the structural model, Fks1 GT domain is located close to the C-terminus of Pbr1. The analysis revealed that all biotinylated lysine residues on Fks1 were localized within the GT domain (*SI Appendix*, Fig. S7*C*), consistent with the predicted model in which the GT domain lies in proximity to the C terminus of Pbr1.

Based on these results, a possible model for the Pbr1–Fks1 interaction is as follows. Pbr1 initially binds to the N-terminal AC domain of Fks1 during the early stages of translation (Fig. 6*C*). As Fks1 elongation and folding proceed, spatial competition with other domains arises. Because Pbr1 coimmunoprecipitates with full-length Fks1, it is likely that Pbr1 remains transiently associated with Fks1 during late stages of Fks1 folding. Ultimately, Pbr1 would dissociate from the AC domain, allowing fully folded Fks1 to be generated.

Structural Basis for Pyridine Nucleotide Recognition by Pbr1. Using AlphaFold3, we assessed the binding stability between Pbr1 and potential cofactors (Fig. 6*D*). NAD (ipTM = 0.95), NADP (ipTM = 0.94), and NADPH (ipTM = 0.94) yielded highly confident interface predictions, whereas heme (ipTM = 0.72) and FAD (ipTM = 0.85) showed lower values, consistent with a structural compatibility between Pbr1 and pyridine nucleotides.

Canonical oxidoreductases have a GxxxGxG nucleotide-binding motif but *S. cerevisiae* Pbr1 contains a Gln residue insertion resulting in the variant sequence GxxxQGxG. This insertion does not appear to interfere with cofactor binding, as the corresponding Gln64 side chain projects away from the diphosphate moiety of NADPH, thereby avoiding steric hindrance (*SI Appendix*, Fig. S7*D*). We constructed single, double, and triple glycine-to-alanine substitutions within this motif and found that they are expressed relatively normally, localized to the ER, although the triple mutant was somewhat compromised for localization, and retained detectable Pbr1 function in vivo; none of these changes markedly lowered the pLDDT score at the NADPH-binding site in the structural model (*SI Appendix*, Fig. S8 *A–E*), suggesting that the Rossmann-like glycine-rich loop of Pbr1 tolerates structural variation in the model.

Beyond this loop, the catalytic pocket also shows notable deviations from canonical oxidoreductases. Although the canonical catalytic Tyr232 is replaced by Phe232, the Lys236 residue within the FxxxK motif still interacts with the hydroxy group of the nicotinamide-linked ribose in the model (*SI Appendix*, Fig. S8*F*). There are examples of functional oxidoreductases known to deviate from the classic YxxxK active site motif (43, 44). To test whether the Pbr1 FxxxK motif has a functional role, we constructed a Lys236-to-Ala236 substitution to generate a FxxxA motif and found that the resultant protein was expressed normally, localized to the ER, and capable of rescuing the lethality of a *pbr1*Δ mutant (*SI Appendix*, Fig. S8 *A–D*). Thus, while Pbr1 retains the overall architecture of oxidoreductases, alterations at the potential key

catalytic residues imply either it lacks catalytic activity or functions with a noncanonical mode of catalysis.

Within the Rossmann-like fold cavity, an unstructured loop spanning Val142–Pro149 crosses the center of the domain (*SI Appendix*, Fig. S8*G*). Ser144 and Gly145 in this loop contact the ribose moieties of the nicotinamide mononucleotide and adenine groups of NADPH, respectively (*SI Appendix*, Fig. S8*F*). The *pbr1-5002* allele substitutes Ser144 with Pro (*SI Appendix*, Fig. S1), and structural modeling shows that this change lowers the pLDDT score at the NADPH-binding site (*SI Appendix*, Fig. S8*H*). Another allele, *pbr1-5006*, carries an S281P substitution (*SI Appendix*, Fig. S1 *B* and *C*) that likewise decreases the predicted confidence of the NADPH-binding region (*SI Appendix*, Fig. S8*H*). These structural changes are predicted to perturb the modeled NADPH-binding region and are consistent with the reduced in vivo function of the *pbr1-5002* and *pbr1-5006* mutants.

At the bottom of the Rossmann-like fold, Met279, Ser281, and Ser283 interact with the nicotinamide and diphosphate groups of NADPH (*SI Appendix*, Fig. S8*F*). The cavity opens toward the membrane surface (Fig. 6*E*), suggesting that the putative substrate of Pbr1 may access the active site directly from the ER membrane. When viewed from the membrane surface, this region reveals a small opening, with the Gln64 residue inserted in the GxxxGxG motif forming part of the rim (Fig. 6*F*). Another opening is also visible at the back of the pocket (Fig. 6*G*). Together, these results suggest that Pbr1 adopts a Rossmann-like fold compatible with pyridine nucleotide binding and functions either as a noncatalytic chaperone or as a noncanonical, oxidoreductase-related factor in ER membrane protein biogenesis.

Discussion

This study assigns a biological process to Pbr1, one of the last uncharacterized essential genes in budding yeast. By combining two unbiased and mechanistically distinct omics strategies, we show that both lines of evidence converge on cell-wall biosynthesis and specifically implicate β-(1,3)-glucan synthesis via *FKS1*. Mechanistically, we demonstrate that Pbr1 is an ER membrane protein with both termini exposed to the cytosol. This topology enables Pbr1 to promote the cotranslational folding and ER maturation of Fks1 in cooperation with Ilm1 and the EMC complex. In *pbr1* mutants, Fks1 becomes ERAC-retained and ERAD-sensitive, and its abundance declines. Pbr1 physically associates with Fks1, and an *fks1-A768D* suppressor allele partially restores Fks1 stability and growth, suggesting that Fks1 folding represents a major essential function of Pbr1. Together, these findings indicate that Pbr1 is a component of the ER folding machinery required for Fks1 biogenesis. Although our data support Fks1 as a major functional client of Pbr1, they do not exclude the possibility that Pbr1 also contributes to the biogenesis or function of additional membrane proteins. A remaining limitation is that we cannot fully distinguish whether the phenotypes of individual *pbr1* ts alleles reflect altered expression, reduced protein stability, allele-specific functional defects, or differences in ERAC formation.

Pbr1 Functions as a Dynamic Folding Scaffold for Fks1 Biogenesis. We envision that Pbr1 dynamically engages nascent Fks1 during its biogenesis at the ER, acting as a folding scaffold that transiently associates with distinct domains as translation proceeds. First, membrane topological analysis indicates that Pbr1 anchors to the cytosolic face of the ER through a short hydrophobic helix, with both termini exposed to the cytosol. Second, AlphaFold3 structural modeling supports this topology and reveals a spatial configuration consistent with Pbr1's predicted membrane orientation. The Rossmann-like fold domain of Pbr1 is positioned to contact the cytosolic N-terminal accessory (AC) domain of Fks1, whereas its C-terminal region lies adjacent to the glycosyltransferase (GT) domain. Third, this interaction model is further supported by TurboID proximity-labeling data. Based on these complementary findings, we propose a sequential binding model in which Pbr1 associates with the AC domain early during translation, maintains transient contact during folding of the TM and GT regions, and releases upon Fks1 maturation. This dynamic association likely enables Pbr1 to monitor the folding trajectory of Fks1 and prevent premature aggregation.

Evolutionary Conservation and Diversification of Pbr1 Orthologs. Comparative analyses reveal that *Pbr1* orthologs across ascomycetes retain the Rossmann-like fold structure but differ in catalytic motifs and cofactor-binding sites.

Candida albicans Pbr1 preserves the canonical YxxxK catalytic motif, whereas *S. pombe* and *S. cerevisiae* variants exhibit substitutions, VxxxK and FxxxK, respectively, lacking a catalytic tyrosine.

This evolutionary diversification suggests that Pbr1 proteins have gradually diverged from canonical short-chain dehydrogenase/reductase (SDR) enzymes toward noncanonical redox or chaperone-like functions. In this context, Pbr1 may represent a unique evolutionary example of an SDR-derived ER factor repurposed for membrane-protein quality control rather than enzymatic catalysis.

Redox Potential and Chaperone-Like Activity of Pbr1. Structural modeling indicates that Pbr1 retains high-affinity binding to pyridine nucleotides (NAD^+/NADH/NADPH) despite its atypical motifs (GxxxQGxG, FxxxK). Notably, oxidoreductases are increasingly recognized to exert noncatalytic functions in proteostasis. For example, PDI family proteins act as ER luminal chaperones and folding sensors that recognize misfolded proteins and facilitate ER-associated degradation, whereas NOQ1 stabilizes client proteins independently of catalytic activity (45–48). Because these characterized noncatalytic functions are typically exerted in the ER lumen or cytosol, Pbr1 may represent a membrane-embedded counterpart, operating at the level of the lipid bilayer.

One plausible scenario is that Pbr1 locally adjusts lipid oxidation or bilayer thickness via NAD(P)H-dependent processes, optimizing the folding environment for Fks1 TM helices. Alternatively, Pbr1 may generate lipophilic metabolites functioning as nonprotein chaperones, analogous to the retinal-mediated stabilization of rhodopsin during its folding (49–51).

Indeed, lipophilic compounds have been shown to rescue misfolded variants of rhodopsin and other multipass membrane proteins such as NPC1 (52–55), suggesting a more general principle in which lipid-derived molecules facilitate membrane-protein folding. Thus, Pbr1 may function as an "SDR-like chaperone," employing a conserved Rossmann-like fold for redox modulation rather than catalysis and thereby linking metabolic redox state to ER proteostasis.

Future Perspectives. Future studies should aim to reconstitute the Pbr1–Fks1 complex in vitro to delineate its folding intermediates and to test whether Pbr1 mediates lipid redox modifications or generates lipophilic cofactors during membrane-protein maturation. A critical next step is to determine whether Pbr1 possesses any oxidoreductase activity through biochemical assays using purified protein. Although we made attempts to purify Pbr1 from several different systems, the protein proved unstable and could not be obtained in soluble form, underscoring the technical challenges of working with this membrane-associated factor.

Investigating *PBR1* orthologs in filamentous and pathogenic fungi could further reveal whether this redox–chaperone mechanism is evolutionarily conserved. Given the essential role of β-(1,3)-glucan synthesis in fungal viability, such studies may highlight ER quality-control factors dedicated to cell-wall biogenesis proteins as novel antifungal targets and have the potential to expand our understanding of how essential ER factors coordinate lipid metabolism with protein biogenesis.

Materials and Methods

Detailed materials and methods are available in *SI Appendix*. This includes the following: yeast strains and media, reagents, genetic manipulation and plasmid construction, morphological profiling of *PBR1*, morphological data acquisition and normalization, similarity and statistical evaluation, immunoblot analysis, cell fractionation, deglycosylation, fluorescence microscopy and data analysis, electron microscopy, in silico analysis of Fks1, integrated membrane yeast two-hybrid (iMYTH), *pbr1-5006* suppressor isolation, *FKS1* suppressor validation, *pbr1*Δ complementation, genetic crosses and tetrad analysis, TurboID analysis, and coimmunoprecipitation.

Data, Materials, and Software Availability. Study data are included in the article and/or *SI Appendix*.

ACKNOWLEDGMENTS. We thank Dr. S. Strahl (Heidelberg University), Dr. A. Nakano (RIKEN), and Dr. H. Nakatogawa (Institute of Science Tokyo), for providing an *O*-glycosylation inhibitor R3A-5a, anti-Sec12 antibody, and a plasmid for N-terminal-tagging with the AID-tag, respectively. We thank Michael Costanzo and Matej Usaj (University of Toronto) for help with *PBR1* genetic network analysis. We thank Jamie Snider and Igor Stagljar (University of Toronto) for reagents and advice with the iMYTH analysis. The AID system was provided by the National Bio-Resource Project of the MEXT (Japan). This work was supported by JSPS KAKENHI [Grant Numbers JP19K06561 (K.O.), JP22K06141 (K.O.), JP23K27126 (T.K.), JP25H01320 (N.N.N.), JP25H01321 (N.N.N.), JP19H03205 (Y.O.), and JP22H02216 (Y.O.)], JSPS Program for Forming Japan's Peak Research Universities (J-PEAKS) [Grant Number JPJS00420240017 (Y.O.)], and the NIH Grants R35GM153501 (E.B.) and R01HG00583 (B.A. and C.B.).

Author affiliations: [a]Department of Biological Science, Graduate School of Science, Nagoya University, Nagoya 464-8602, Japan; [b]Department of Integrated Biosciences, Graduate School of Frontier Sciences, The University of Tokyo, Kashiwa 277-8562, Japan; [c]Department of Cell and Developmental Biology, Perelman School of Medicine at the University of Pennsylvania, Philadelphia, PA 19104-6058; [d]Terrence Donnelly Centre for Cellular and Biomolecular Research and Department of Molecular Genetics, University of Toronto, Toronto, ON M5S 3E1, Canada; [e]Molecular Ligand Target Research Team, RIKEN Center for Sustainable Resource Science, Wako 351-0198, Japan; [f]Molecular Structure Center, World Premier International Research Center Initiative-Institute of Transformative Bio-Molecules, Nagoya University, Nagoya 464-8602, Japan; [g]Faculty of Science, Yamagata University, Yamagata 990-8560, Japan; [h]Institute for Integrated Cell-Material Sciences, Kyoto University, Kyoto 606-8501, Japan; [i]Center for Integrative Genomics, Quartier UNIL-Sorge Bâtiment Génopode, Lausanne CH-1015, Switzerland; [j]Department of Systems Biology, UMass Chan Medical SchoolAlbert Sherman Center, 368 Plantation Street, AS6-1059 Worcester, MA 01605; [k]Institute for Genetic Medicine, Hokkaido University, Sapporo 060-0815, Japan; [l]Department of Science and Technology Innovation, Nagaoka University of Technology, Nagaoka 940-2188, Japan; and [m]Collaborative Research Institute for Innovative Microbiology, The University of Tokyo, Tokyo 113-8657, Japan

Author contributions: K.O., J.v.L., B.A., E.B., N.N.N., C.B., and Y.O. designed research; K.O., H. Okada, G.T., G.S., H. Ohtake, K.K., S.I., A.O., E.M.-S., and K.S. performed research; S.O., K.K., Y.Y., Y.T., and T.K. contributed new reagents/analytic tools; F.G., R.A., and Y.I. analyzed data; and K.O., H. Okada, J.v.L., B.A., E.B., N.N.N., C.B., and Y.O. wrote the paper.

1. H. Fujita, Y. Kida, M. Hagiwara, F. Morimoto, M. Sakaguchi, Positive charges of translocating polypeptide chain retrieve an upstream marginal hydrophobic segment from the endoplasmic reticulum lumen to the translocon. *Mol. Biol. Cell* **21**, 2045–2056 (2010).
2. G. Gafvelin, G. von Heijne, Topological "frustration" in multispanning E. coli inner membrane proteins. *Cell* **77**, 401–412 (1994).
3. G. Heijne, The distribution of positively charged residues in bacterial inner membrane proteins correlates with the trans-membrane topology. *EMBO J.* **5**, 3021–3027 (1986).
4. M. Higy, T. Junne, M. Spiess, Topogenesis of membrane proteins at the endoplasmic reticulum. *Biochemistry* **43**, 12716–12722 (2004).
5. J. P. Chapple *et al.*, Unfolding retinal dystrophies: A role for molecular chaperones? *Trends Mol. Med.* **7**, 414–421 (2001).
6. M. E. Gelsthorpe *et al.*, Niemann-Pick type C1 I1061T mutant encodes a functional protein that is selected for endoplasmic reticulum-associated degradation due to protein misfolding. *J. Biol. Chem.* **283**, 8229–8236 (2008).
7. P. Kim Chiaw, P. D. Eckford, C. E. Bear, Insights into the mechanisms underlying CFTR channel activity, the molecular basis for cystic fibrosis and strategies for therapy. *Essays Biochem.* **50**, 233–248 (2011).
8. A. W. Partridge, A. G. Therien, C. M. Deber, Polar mutations in membrane proteins as a biophysical basis for disease. *Biopolymers* **66**, 350–358 (2002).
9. C. R. Sanders, J. K. Myers, Disease-related misassembly of membrane proteins. *Annu. Rev. Biophys. Biomol. Struct.* **33**, 25–51 (2004).
10. M. Tector, F. U. Hartl, An unstable transmembrane segment in the cystic fibrosis transmembrane conductance regulator. *EMBO J.* **18**, 6290–6298 (1999).
11. X. Hu *et al.*, Structural and mechanistic insights into fungal beta-1,3-glucan synthase FKS1. *Nature* **616**, 190–198 (2023).
12. S. B. Inoue *et al.*, Characterization and gene cloning of 1,3-beta-D-glucan synthase from Saccharomyces cerevisiae. *Eur. J. Biochem.* **231**, 845–854 (1995).
13. Z. Ren *et al.*, Structural basis of fungal beta-1,3-glucan synthase inhibition by caspofungin. *Nature* **654**, 547–555 (2026), 10.1038/s41586-026-10409-7.
14. R. S. Hegde, R. J. Keenan, The mechanisms of integral membrane protein biogenesis. *Nat. Rev. Mol. Cell Biol.* **23**, 107–124 (2022).
15. M. J. Shurtleff *et al.*, The ER membrane protein complex interacts cotranslationally to enable biogenesis of multipass membrane proteins. *Elife* **7**, e37018 (2018).
16. M. C. Jonikas *et al.*, Comprehensive characterization of genes required for protein folding in the endoplasmic reticulum. *Science* **323**, 1693–1697 (2009).
17. Y. Ohya *et al.*, High-dimensional and large-scale phenotyping of yeast mutants. *Proc. Natl. Acad. Sci. U.S.A.* **102**, 19015–19020 (2005).
18. F. Ghanegolmohammadi *et al.*, Systematic analysis of Ca(2+) homeostasis in Saccharomyces cerevisiae based on chemical-genetic interaction profiles. *Mol. Biol. Cell* **28**, 3415–3427 (2017).
19. J. A. Shaw *et al.*, The function of chitin synthases 2 and 3 in the Saccharomyces cerevisiae cell cycle. *J. Cell Biol.* **114**, 111–123 (1991).
20. Z. Hong *et al.*, Cloning and characterization of KNR4, a yeast gene involved in (1, 3)-β-glucan synthesis. *Mol. Cell. Biol.* **14**, 1017–1025 (1994).
21. M. Costanzo *et al.*, A global genetic interaction network maps a wiring diagram of cellular function. *Science* **353** (2016).
22. J. van Leeuwen *et al.*, Exploring genetic suppression interactions on a global scale. *Science* **354** (2016).
23. A. F. Ram, A. Wolters, R. Ten Hoopen, F. M. Klis, A new approach for isolating cell wall mutants in Saccharomyces cerevisiae by screening for hypersensitivity to calcofluor white. *Yeast* **10**, 1019–1030 (1994).
24. C. Roncero, M. H. Valdivieso, J. C. Ribas, A. Duran, Isolation and characterization of Saccharomyces cerevisiae mutants resistant to Calcofluor white. *J. Bacteriol.* **170**, 1950–1954 (1988).
25. A. Turchini, L. Ferrario, L. Popolo, Increase of external osmolarity reduces morphogenetic defects and accumulation of chitin in a gas1 mutant of Saccharomyces cerevisiae. *J. Bacteriol.* **182**, 1167–1171 (2000).
26. G. Huyer *et al.*, A striking quality control subcompartment in Saccharomyces cerevisiae: The endoplasmic reticulum-associated compartment. *Mol. Biol. Cell* **15**, 908–921 (2004).
27. J. Arroyo *et al.*, Functional and genomic analyses of blocked protein O-mannosylation in baker's yeast. *Mol. Microbiol.* **79**, 1529–1546 (2011).
28. M. G. Orchard *et al.*, Rhodanine-3-acetic acid derivatives as inhibitors of fungal protein mannosyl transferase 1 (PMT1). *Bioorg. Med. Chem. Lett.* **14**, 3975–3978 (2004).
29. C. Xu, S. Wang, G. Thibault, D. T. Ng, Futile protein folding cycles in the ER are terminated by the unfolded protein O-mannosylation pathway. *Science* **340**, 978–981 (2013).
30. A. Helenius, M. Aebi, Roles of N-linked glycans in the endoplasmic reticulum. *Annu. Rev. Biochem.* **73**, 1019–1049 (2004).
31. H. Okada, S. Ohnuki, C. Roncero, J. B. Konopka, Y. Ohya, Distinct roles of cell wall biogenesis in yeast morphogenesis as revealed by multivariate analysis of high-dimensional morphometric data. *Mol. Biol. Cell* **25**, 222–233 (2014).
32. M. E. Johnson, T. D. Edlind, Topological and mutational analysis of Saccharomyces cerevisiae Fks1. *Eukaryot. Cell* **11**, 952–960 (2012).
33. K. Nishimura, T. Fukagawa, H. Takisawa, T. Kakimoto, M. Kanemaki, An auxin-based degron system for the rapid depletion of proteins in nonplant cells. *Nat. Methods* **6**, 917–922 (2009).
34. S. Ghaemmaghami *et al.*, Global analysis of protein expression in yeast. *Nature* **425**, 737–741 (2003).
35. W. K. Huh *et al.*, Global analysis of protein localization in budding yeast. *Nature* **425**, 686–691 (2003).
36. M. Meurer *et al.*, Genome-wide C-SWAT library for high-throughput yeast genome tagging. *Nat. Methods* **15**, 598–600 (2018).
37. U. Weill *et al.*, Genome-wide SWAp-Tag yeast libraries for proteome exploration. *Nat. Methods* **15**, 617–622 (2018).
38. I. Yofe *et al.*, One library to make them all: Streamlining the creation of yeast libraries via a SWAp-Tag strategy. *Nat. Methods* **13**, 371–378 (2016).
39. K. Iyer *et al.*, Utilizing the split-ubiquitin membrane yeast two-hybrid system to identify protein-protein interactions of integral membrane proteins. *Sci. STKE* **2005**, pl3 (2005).
40. B. L. Greenwood, K. Oshima, D. T. Stuart, Integrated membrane yeast two-hybrid system for the analysis of membrane protein complexes. *Bio. Protoc.* **15**, e5418 (2025).
41. J. Abramson *et al.*, Addendum: Accurate structure prediction of biomolecular interactions with AlphaFold 3. *Nature* **636**, E4 (2024).
42. T. C. Branon *et al.*, Efficient proximity labeling in living cells and organisms with TurboID. *Nat. Biotechnol.* **36**, 880–887 (2018).
43. Y. Kallberg, U. Oppermann, H. Jornvall, B. Persson, Short-chain dehydrogenases/reductases (SDRs). *Eur. J. Biochem.* **269**, 4409–4417 (2002).
44. K. L. Kavanagh, H. Jornvall, B. Persson, U. Oppermann, Medium- and short-chain dehydrogenase/reductase gene and protein families: The SDR superfamily: Functional and structural diversity within a family of metabolic and regulatory enzymes. *Cell Mol. Life Sci.* **65**, 3895–3906 (2008).
45. G. Asher, J. Lotem, B. Cohen, L. Sachs, Y. Shaul, Regulation of p53 stability and p53-dependent apoptosis by NADH quinone oxidoreductase 1. *Proc. Natl. Acad. Sci. U.S.A.* **98**, 1188–1193 (2001).
46. G. Asher *et al.*, P53 hot-spot mutants are resistant to ubiquitin-independent degradation by increased binding to NAD(P)H:Quinone oxidoreductase 1. *Proc. Natl. Acad. Sci. U.S.A.* **100**, 15065–15070 (2003).

47. F. Hatahet, L. W. Ruddock, Protein disulfide isomerase: A critical evaluation of its function in disulfide bond formation. *Antioxid. Redox Signal.* **11**, 2807–2850 (2009).
48. B. Wilkinson, H. F. Gilbert, Protein disulfide isomerase. *Biochim. Biophys. Acta* **1699**, 35–44 (2004).
49. S. Kaushal, H. G. Khorana, Structure and function in rhodopsin. 7. Point mutations associated with autosomal dominant retinitis pigmentosa. *Biochemistry* **33**, 6121–6128 (1994).
50. C. H. Sung, C. M. Davenport, J. Nathans, Rhodopsin mutations responsible for autosomal dominant retinitis pigmentosa. Clustering of functional classes along the polypeptide chain. *J. Biol. Chem.* **268**, 26645–26649 (1993).
51. C. H. Sung, B. G. Schneider, N. Agarwal, D. S. Papermaster, J. Nathans, Functional heterogeneity of mutant rhodopsins responsible for autosomal dominant retinitis pigmentosa. *Proc. Natl. Acad. Sci. U.S.A.* **88**, 8840–8844 (1991).
52. T. Li *et al.*, Effect of vitamin A supplementation on rhodopsin mutants threonine-17 –> methionine and proline-347 –> serine in transgenic mice and in cell cultures. *Proc. Natl. Acad. Sci. U.S.A.* **95**, 11933–11938 (1998).
53. S. M. Noorwez *et al.*, Pharmacological chaperone-mediated in vivo folding and stabilization of the P23H-opsin mutant associated with autosomal dominant retinitis pigmentosa. *J. Biol. Chem.* **278**, 14442–14450 (2003).
54. K. Ohgane, K. Dodo, Y. Hashimoto, Retinobenzaldehydes as proper-trafficking inducers of folding-defective P23H rhodopsin mutant responsible for retinitis pigmentosa. *Bioorg. Med. Chem.* **18**, 7022–7028 (2010).
55. K. Ohgane, F. Karaki, K. Dodo, Y. Hashimoto, Discovery of oxysterol-derived pharmacological chaperones for NPC1: Implication for the existence of second sterol-binding site. *Chem. Biol.* **20**, 391–402 (2013).